Chenhua Zhao
Juming Yao
Hiromi Masuda
Raghuvansh Kishore*
Tetsuo Asakura
Department of Biotechnology, Tokyo University of Agriculture and Technology, Koganei, Tokyo 184-8588, Japan

Received 5 March 2002; accepted 11 November 2002

Structural Characterization and Artificial Fiber Formation of *Bombyx mori* Silk Fibroin in Hexafluoro-Iso-Propanol Solvent System

Abstract: *High-resolution solution ^{13}C-NMR and CD studies of* Bombyx mori *silk fibroin revealed the presence of an ordered secondary structure 3_{10}-helix, in hexafluoro-iso-propanol (HFIP). The solid-state structure of the silk fibroin film prepared by drying it gently from the HFIP solution still keep the structure, 3_{10}-helix, which was studied with high-resolution solid state ^{13}C-NMR. The structural transition from the 3_{10}-helix to silk II structure, heterogeneous structure including antiparallel β-sheet, occurred during the artificial spinning from the HFIP solution. The wide-angle x-ray diffraction and differential scanning calorimetry thermograms of the artificial spinning fiber after postspinning treatments were observed together with the stress–strain curves. The results emphasize that the molecular structures, controlled morphology, and mechanical properties of the protein-based synthetic polymers can be modulated for enhancing biocompatibility.* © 2003 Wiley Periodicals, Inc. Biopolymers 69: 253–259, 2003

Keywords: Bombyx mori *silk fibroin; hexafluoro-iso-propanol; ^{13}C CP/MAS NMR; 3_{10}-helix; ^{13}C chemical shift*

INTRODUCTION

Silk proteins are of practical interest because of their excellent intrinsic properties utilizable in biotechnological and biomedical fields as well as the importance of silkworm silks in the manufacture of high-quality textiles.[1–5] Moreover, moderate quantities of silks and silk-mimic biopolymers have been achieved due to the advances in molecular biotechnology and protein engineering.[6–8] However, production of useful materials, such as fibers, from these potential supplies of unprocessed biopolymers requires a detailed understanding of processing conditions necessary to induce the hierarchical structure responsible for the outstanding mechanical properties exhibited by native silk fibers, of the relationship among the protein primary structure, molecular self-assembly, and the microstructure, which may provide some control over the complex spinning mechanism of the silk fibers. So the final hurdle on the way to the production

Correspondence to: Tetsuo Asakura; email: asakura@cc.tuat.ac.jp
*On leave from the Institute of Microbial Technology, Sector 39-A, Chandigarh—160 036, India
Biopolymers, Vol. 69, 253–259 (2003)

of man-made silks now lies in the development of an appropriate spinning technology capable of converting these raw materials into high-performance fibers. It is advantageous to focus on the regeneration of natural silks and their structural information in the spinning process because these can be used as a benchmark for evaluating the success of the spinning process.

A number of groups have attempted to spin silk protein fibers, most involving regenerated *Bombyx mori* silk[9–14] or spider silk.[15] Since the fiber properties depend on the conditions under which they have been obtained, the nature of the solvent and the postspinning treatments applied to the fibers may be the important factors, affecting the overall quality and properties of the fibers produced. To date, both hexafluoro-iso-propanol (HFIP)[9–11] and hexafluoroacetone hydrate (HFA · hydrate)[12] have been proposed as useful solvents for the regeneration of the silk fibroins. However, there is lack of structural information on the silk fibroins in such solvent systems, especially the structural transition is still not clear during the spinning process.

Here, we presented a detailed investigation of the effect of HFIP solvent on the molecular structure of *B. mori* silk fibroin before and after artificial spinning by using NMR and CD measurements. The characterization of the regenerated silk fibers was performed by using stress–stain curves, wide-angle x-ray diffraction (WAXD), and differential scanning calorimetry (DSC). The knowledge of the structure of fibroin molecule and its manipulation may turn out to be useful to approach artificial spinning of the silk fibers of desired functionalities.

MATERIALS AND METHODS

Bombyx mori Regenerated Silk Film

In order to prepare regenerated silk fibroin, *B. mori* cocoons were degummed twice with 0.5% (w/v) Marseilles soap solution at 100°C for 30 min and washed thoroughly with distilled water to remove silk sericin. The fibroin fibers were then dissolved in 9*M* LiBr (Wako Pure Chemical Industries, Ltd.) solution at 40°C for about 30 min. After extensive dialysis against distilled water for four days, the aqueous solution was "gently" evaporated by forced airflow to a concentration of about 2% (w/v). The fibroin film was prepared by spreading the concentrated aqueous solution over a poly(methyl methacrylate) plate and left it for drying at 25°C. This form of "film" is termed as aqueous silk fibroin film and used directly for observing the solid-state ^{13}C cross-polarization/magic angle spinning (CP/MAS) NMR and CD spectra in fluorinated solvents.

Artificial Spinning

The HFIP solution of *B. mori* silk fibroin at 10% (w/w) was transferred to a pump fitted with a stainless steel screens (80 mesh), as reported previously.[12] The viscosity of all the solution at 50% radian was 18.3 poise determined with a mechanical spectrometer (RMS-800, Rheometric Far East Ltd., Japan). The solution was extruded employing high-pressure nitrogen gas through a stainless steel spinneret (diameter of 0.2 mm, length of 1.2 mm). The methanol was used as the coagulant. The as-spun filament traveled through an air space of 2.0 cm before achieving coagulation. To allow the diffusion of entrapped HFIP solvent molecules from the fibers, the extruded filaments were soaked overnight in methanol. In order to improve the mechanical properties, the filaments were then drawn to 3 times its original length in distilled water and steam-annealed at 125°C for 30 min. The fibers, after the postspinning treatments, were immobilized on the bobbins to prevent recoiling and then allowed to dry overnight at room temperature.

NMR Measurements

The solid-state ^{13}C CP/MAS NMR spectra of *B. mori* silk fibroin were recorded at 25°C on a Chemagnetics CMX 400 spectrometer operating at 100 MHz with a 4 ϕ mm cylindrical rotor. The typical sample spinning speed was 10 kHz, with a spectral width of 40 kHz and data points of 32K. The numbers of scans were 8–15K. A ^{1}H 90° pulse of 4 μs, contact time of 1 ms, and a pulse delay of 5 s were employed. The corrected ^{13}C chemical shifts are reported (in ppm) with respect to adamantane methyl peak observed at 28.8 ppm, relative to standard tetramethylsilane (TMS), described previously.[16]

The solution-state ^{13}C-NMR spectrum of *B. mori* silk fibroin in HFIP was recorded at 25°C on a JEOL α-500 spectrometer operating at 125 MHz. The 45° pulse with acquisition time of 0.97 s and delay time of 2.5 s was used for observation. The spectral width was 34K Hz with the data points of 32K. Up to 20K scans were accumulated. The chemical shifts were recorded with TMS as an internal reference. The sample concentration was 4% (w/w) and a small amount of D_2O (5%) was added to the solution.

CD Measurements

CD pattern of the regenerated silk fibroin film dissolved in HFIP was measured between 185 and 260 nm with a JASCO J-805 spectropolarimeter. The measurement was made at room temperature using a quartz cell with path length of 0.1 mm. The reported CD pattern represents an average of eight consecutive scans, measured at 1 nm a resolution. The instrument was continuously flushed with dry nitrogen gas. The molar ellipticity $[\theta]_M$ values are determined by taking into account the molecular weight of 391 kDa with amino acid residues of 5263, reported for *B. mori* fibroin protein.[2,17]

Wide-Angle X-Ray Diffraction

The structural analyses of the *B. mori* fiber were performed using WAXD experiments on a RINT-2400 Rigaku fine-focus fixed tube generator with Ni-filtered CuK_α radiation and a flat film camera with pinhole collimation. The voltage and current of the x-ray source were 40 kV and 100 mA, respectively. Well-aligned fiber bundles of *B. mori* native fibroin fibers and the regenerated fibroin fibers from HFIP system were mounted vertically at the exist of the collimator. The Si and Ni standard were used for calibration. The typical camera lengths were 1.8 or 3 cm. The WAXD patterns were observed by rotating the samples along the fiber axis at the intense Bragg reflection near $2\theta = 19.8°$.

Differential Scanning Calorimetry

DSC measurements were performed on a Rigaku Thermoflex (DSC8230D) (Rigaku Denki Co., Ltd. Japan), in the range of 30–350°C, at the uniform heating rate of 10°C/min. The sample weight and DSC range were 2.7 mg and 2 mcal/s, respectively. An open aluminium pan was swept with N_2 gas during the course of heating process.

Mechanical Properties.

The mechanical properties of the artificially spun silk fibers and native fibers were measured using a Tensilon tensile testing machine (RTM-100) operating at 20°C at the relative humidity of 65%. The Young's modulus is calculated by taking into account the initial slopes of the lines in the graph. Before analysis the samples were equilibrated in a controlled environment for at least 24 h. The rate of crosshead was 50 mm/min on samples of 90 mm length with chart speed of 500 mm/min. Each value reported represents an average of fifteen consecutive measurements.

RESULTS AND DISCUSSION

Silk Fibroins Before Structural Transition

In ^{13}C-NMR structural analyses of *B. mori* and Samia cynthia ricini (*S. c. ricini*) silk fibroins, the three crystalline forms—namely, silk I (before spinning), silk II (after spinning), and α-helix—have been distinguished by the conformation-dependent ^{13}C chemical shifts of the respective amino acid residues.[18–20] Before we describe the results of our findings on the artificial spinning, it would be of interests to perform the structural analysis of *B. mori* silk fibroin films in HFIP solvent system, in the solid state as well as in the solution state. The solid-state ^{13}C CP/MAS NMR spectra of *B. mori* silk fibroin films prepared from the aqueous and HFIP solutions are shown in Figure 1(a) and (b), respectively. The characteristic chemical shifts from different *B. mori* silk fibroin samples arising from the predominant Gly (42.9%), Ala (30.0%), and Ser (12.2%) residues are listed in Table I. The resonance assignments are readily made on the basis of published solid-state ^{13}C-NMR chemical shift data of silk fibroins and the model peptides.[12,16,18–20] The observed ^{13}C-NMR chemical shifts and the broad line shape of the peaks in Figure 1(a) suggest that *B. mori* silk fibroin takes random coil structure in the film prepared here from the aqueous solution. However, the characteristic resonance, especially the Ala C_β at 15.2 ppm and Ala C_α at 52.4 ppm in Figure 1(b), suggests that the residues strongly favor an ordered structure, most likely helical structure, in *B. mori* silk fibroin film prepared from the HFIP solution. This is

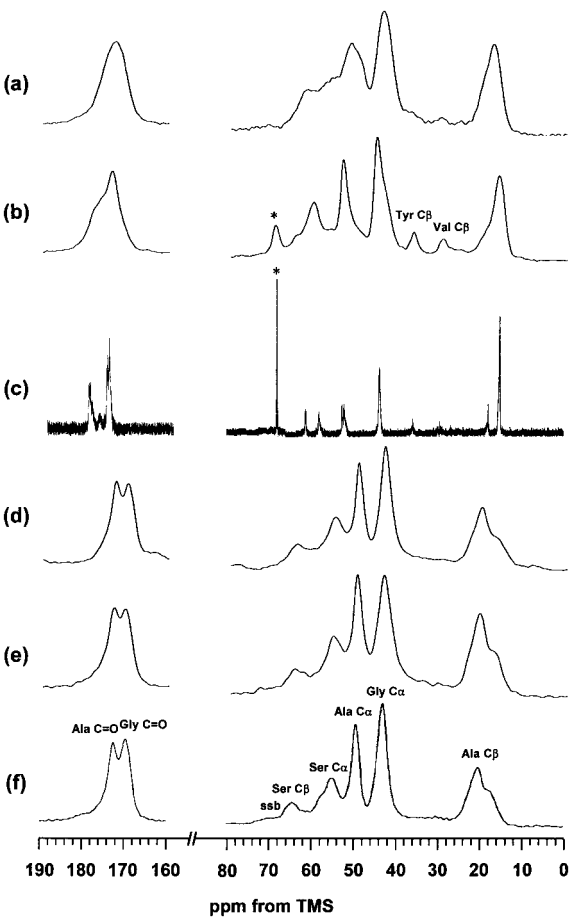

FIGURE 1 ^{13}C-NMR spectra of (a) *B. mori* silk fibroin film prepared from the aqueous solution, (b) *B. mori* silk fibroin film prepared from the HFIP solution, (c) *B. mori* silk fibroin in HFIP solution, (d) as-spun regenerated *B. mori* silk fibroin fiber, (e) regenerated *B. mori* silk fibroin fiber after postspinning treatments (drawing ratio, ×3, and steam annealing at 125°C for 30 min), and (f) native *B. mori* silk fibroin fiber. The peak assignments are shown in the spectra, (b) and (f). Asterisk indicates the HFIP peak and ssb means spinning side band.

Table I Characteristic ^{13}C CP/MAS NMR Chemical Shifts (in ppm) Arising from the Predominant Amino Acid Residues of *B. mori* Silk Fibroin Samples After Different Treatments

	(a)[a] Silk Film (9*M* LiBr and Water Dialysis)	(b) Film from HFIP Solution	(c) Silk–HFIP Solution	(d) Regenerated Silk Fibroin Fiber (As-Spun)	(e) Regenerated Silk Fibroin Fiber (×3, Steam Annealing at 125°C for 30 min)	(f) Natural Silk Fiber
Gly C_α	43.0	44.3	43.8	42.6	42.7	42.5
Gly CO	170.9	172.7	173.4	169.4	169.6	169.3
Ala C_α	50.4	52.4	52.7	48.9	48.9	48.9
			52.2			
Ala C_β	16.6	15.2	15.1	17.1	17.0	16.7
				20.1	20.2	19.9
				22.6	22.6	22.1
Ala CO	—	—	177.9	172.1	172.4	172.2
Ser C_α	—	59.4	58.1	54.4	54.9	54.6
Ser C_β	—	—	61.2	63.2	64.1	63.9

[a] (a)–(f) corresponds to Figure 1(a)–(f).

because the chemical shifts of Ala C_β and Ala C_α were 15.7 and 52.5 ppm, respectively, for the silk proteins in a typical α-helix structure, which was significantly different from these in other structures.[20] In order to check whether there is a structural transition during the film preparation process, a solution-state ^{13}C-NMR spectrum was observed for *B. mori* silk fibroin in the HFIP solution, as shown in Figure 1(c). The corresponding chemical shifts are also listed in Table I, according to the peak assignments reported previously.[21] The chemical shift data are the same between Figure 1(b) and (c), suggesting that there is no structural transition during the film preparation.

To further characterize the conformational features of the silk fibroin in the HFIP solution, the CD pattern of *B. mori* silk fibroin in the HFIP solution was recorded at a concentration of 2.56 μM, as shown in Figure 2. The CD pattern is characterized by the presence of two negative bands: a weak shoulder at 222 nm and a relatively stronger band at 205 nm and a distinct strong positive extreme at 191 nm with a crossover at 197 nm. These results provide strong evidence that the fibroin conformation, in a specific hydrophobic environment, is predominantly a kind of helical structure, not random coil. By considering the characteristic ratio R of 3_{10}-helix structure,[22,23] we assigned this spectral feature to a 3_{10}-helix structure as judged from the ratio $R = [\theta]_{222}/[\theta]_{205} = 0.5$. A similar CD pattern in HFIP has been reported for high-molecular weight poly-L-Ala and has been ascribed to a "distorted" α-helical conformation by Parrish et al.[24] As they suggested, the proposed "distorted helical structure" is stabilized by an additional hydrogen bond involving the backbone amide C=O and the OH group of HFIP molecule consequently, referred as a "doubly hydrogen-bonded helix." Here, it must be noted that the torsional angles ϕ and ψ reported by these authors are very close to these of the 3_{10}-helical structure.

Silk Fibroins After Structural Transition Monitored with ^{13}C CP/MAS NMR

Figure 1(d) and (e) show ^{13}C CP/MAS NMR spectra of the regenerated *B. mori* silk fibers prepared from

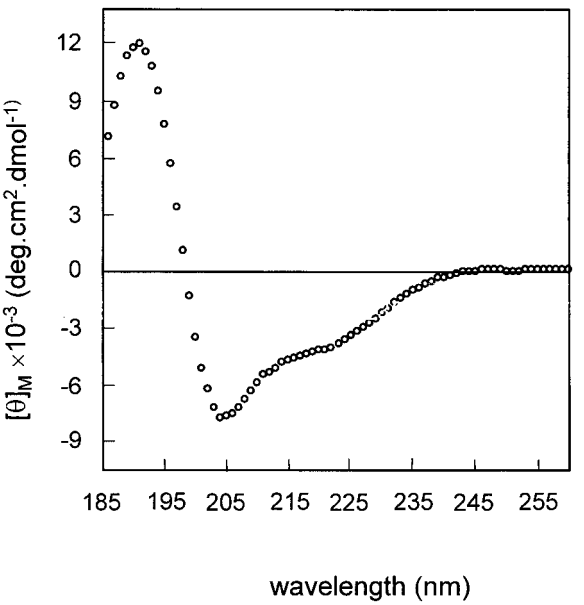

FIGURE 2 CD pattern of *B. mori* silk fibroin dissolved in HFIP. The concentration was 2.56 μM.

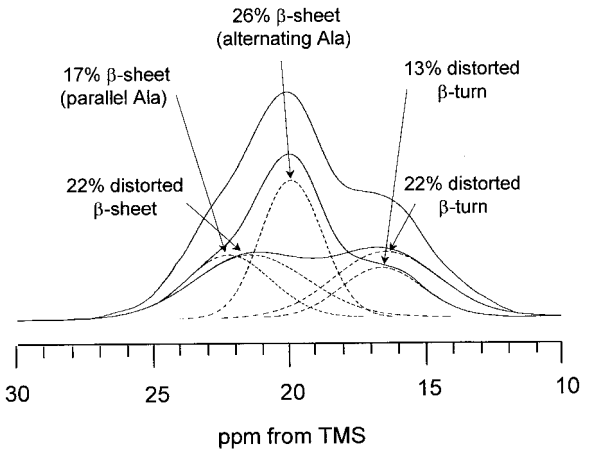

FIGURE 3 Expanded Ala C_β peak of ^{13}C CP/MAS NMR spectrum of the regenerated *B. mori* silk fibroin fiber after postspinning treatments (drawing ratio, ×3, and steam annealing at 125°C for 30 min). The spectral deconvolution was performed by assuming Gaussian. The detailed peak assignment was reported previously.[27,28]

the HFIP solution before and after postspinning treatments, respectively. The corresponding chemical shifts are also summarized in Table I. The ^{13}C chemical shifts of two regenerated silk fibers are similar with that of the native *B. mori* silk fiber [Figure 1(f)]. In both spectra (d) and (e), no peak from HFIP was observed, indicating that the HFIP molecules were eliminated before postspinning treatments. Moreover, the Val C_β and Tyr C_β peaks did not appear clearly in the regenerated silk fibers as well as the native silk fiber, suggesting that the crystal size becomes larger. Previously, we demonstrated that the side chain mobility depends on the local packing density around amino acid residues by using solid state ^2H-NMR.[25] Because of the enlargement of crystal size, the silk fibroin domain containing Tyr and Val residues seems to be incorporated into the relatively tightly packed domain, which consists of $(Gly–Ala–Gly–Ser–Gly–Ala)_n$.[2,26,27]

Among these ^{13}C peaks, the Ala C_β peak is sensitive to both the conformation and intermolecular arrangement. We have clarified the presence of the heterogeneous structure of native fiber from *B. mori* silk fibroin from the ^{13}C CP/MAS NMR analysis of Ala C_β carbon.[26,27] The relative proportions of the various heterogeneous structural components were determined from their relative peak intensities after detailed line-shape deconvolution of the broad and asymmetric Ala C_β peak, coupled with ab initio molecular orbital calculation. In this research, the same analysis was performed to clarify the detailed structure of the regenerated *B. mori* silk fibers. Figure 3 shows the expanded Ala C_β peak in the ^{13}C CP/MAS NMR spectrum of regenerated silk fiber after postspinning drawing (×3, steam annealed at 125°C for 30 min). This regenerated silk fiber contains 13% *distorted* β-turn, 17% β-sheet (parallel Ala residues), and 26% β-sheet (alternating Ala residues), which form the 56% crystalline fraction (mainly repeated Gly–Ala–Gly–Ser–Gly–Ala sequences). The remaining fraction of 44% amorphous Tyr-rich region is formed with 22% in both *distorted* β-turn and *distorted* β-sheet. The similar data were obtained for the as-spun regenerated silk fiber (data not shown). Such a heterogeneous structure is also very similar with that for native *B. mori* silk fibroin fiber,[26,27] suggesting that there is a similar structural character between the regenerated silk fibers and the native silk fiber.

WAXD Measurements

The crystalline structure of the regenerated silk fibroin fibers obtained from HFIP was examined using WAXD measurements. Figure 4 shows the WAXD patterns of the regenerated *B. mori* fibroin fibers obtained from the HFIP solution (a) and the native *B. mori* silk fibroin fiber (b), indicating the distribution of the fiber orientation at an intense broad Bragg reflection near $2\theta = 19.8°$ (crystalline spacing of 4.43 Å). A characteristic feature of silk fibroin fiber with β-sheet structure is shown.[28] The striking similarities between the two WAXD profiles strongly suggest the similarities in the crystal structures of the silk fibers prepared from HFIP solution and the aqueous solution.

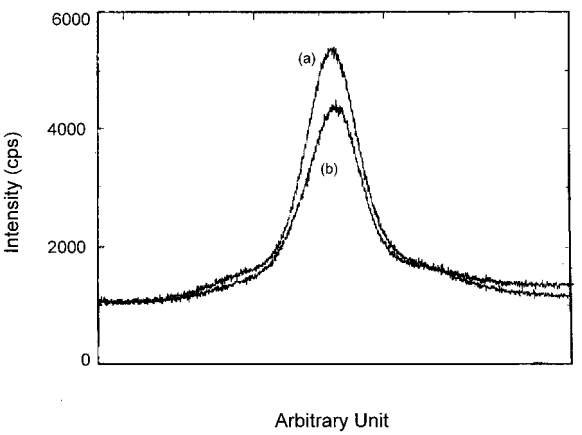

FIGURE 4 WAXD patterns of (a) regenerated *B. mori* silk fibroin fiber after postspinning treatments (drawing ratio, ×3, and steam annealing at 125°C for 30 min) and (b) native *B. mori* silk fibroin fiber. The experimental conditions are described in the text.

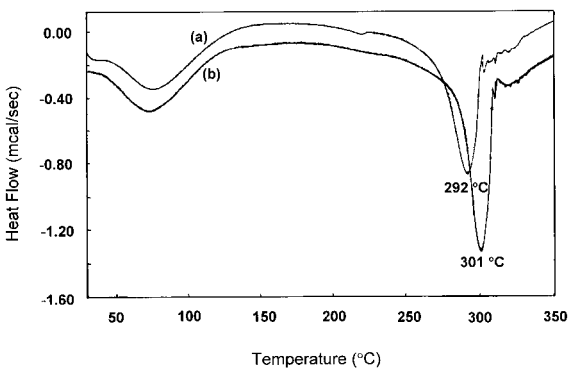

FIGURE 5 DSC curves of regenerated *B. mori* silk fibroin fibers after post-spinning treatments [drawing ratio, ×3, (a) without steam-annealing, and (b) with steam annealing at 125°C for 30 min] on proceeding from 30 to 350°C.

DSC Measurements

Figure 5 shows the DSC thermograms of regenerated silk fibroin fibers with and without steam-annealing after postspinning drawing. The DSC curves displayed two endothermic peaks, one at around 70°C is due to loss of water, and another is both at 292 and 301°C, respectively, which are attributed to the thermal decomposition of fibers.[29] After steam-annealing at 125°C [Figure 5(b)], the DSC curve of the regenerated silk fiber showed a remarkable upward shift of the decomposition temperature by 9°C. The well-oriented silk fibers usually exhibit a decomposition peak at above 300°C.[29] Thus, the silk fiber after steam annealing is similar to the native fiber from viewpoint of thermal character.

Stress–Strain Curves

Figure 6 shows the stress–strain curves of the regenerated *B. mori* silk fibroin fibers prepared from HFIP system with different postspinning treatments [(b)–(d)]. The stress-strain curve of native *B. mori* silk fibroin fiber [curve (a)] is also shown for a comparison, which has the Young's modulus of 5.0 Gpa as calculated from the slope. The results clearly indicate that the Young's modulus, as well as the strength and elasticity, for the regenerated silk fibers after steam annealing, increases to 3.6, 4.3, and 4.7 GPa in Figure 6(e), (d), and (b) for the regenerated silk fibers with the drawing ratios of 1 time, 2 times, and 3 times, respectively. The overall mechanical properties of the spun fibers were improved with increasing the drawing ratios. Additionally, a significant increase in Young's modulus was also observed when the spun fibers from the HFIP solution were treated with the steam annealing [Figure 6(b) with Figure 6(c)], where the regenerated silk fiber without steam annealing after drawing [Figure 6(c)], has the Young's modulus of 4.5 GPa. The mechanical properties of the fibers depend on the crystallinity and degree of molecular orientation. Both NMR data and WAXD patterns reveal the structural similarity between the regenerated *B. mori* silk fibroin fiber after postspinning treatments (drawing ratio, ×3, and steam annealing at 125°C for 30 min) and native silk fiber, suggesting that the regenerated silk fiber were well crystallized and well oriented to the fiber axis after artificial spinning and then postspinning treatments. Note that the size of this regenerated silk fiber is about 15–25 denier, while that for native *B. mori* silk fibroin fiber is about 1–2 denier. Liivak et al.[10] found that there is a linear relationship between the logarithm of the maximum stress sustained by the fibers and the fiber size, and the regenerated fibers with the finest size approach the maximum stress measured for native *B. mori* silk fiber.

CONCLUSION

In this investigation we attempted to characterize the preferred conformation of *B. mori* silk fibroin in a hexafluorinated solvent HFIP shown to have potential

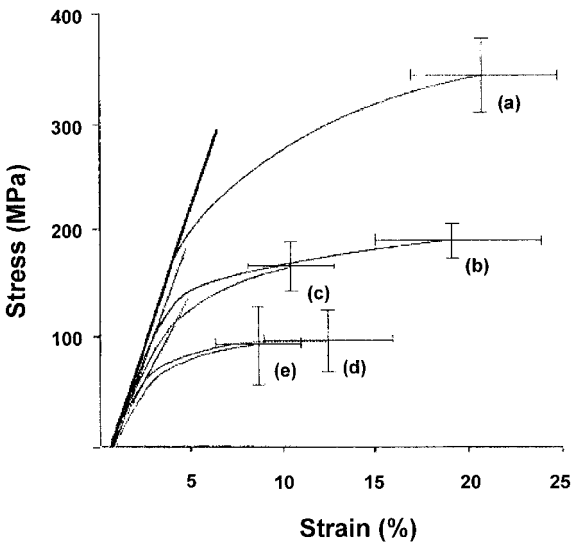

FIGURE 6 Stress–stain curves of (a) native *B. mori* silk fibroin fiber, and (b)–(e) regenerated *B. mori* silk fibroin fibers after postspinning treatments. The curve (b) drawing ratio, ×3, and steam annealing at 125°C for 30 min; (c) drawing ratio, ×3, without steam annealing; (d) drawing ratio, ×2, and steam annealing at 125°C for 30 min; and (e) without drawing, and steam annealing at 125°C for 30 min. The cross signs represent the experimental errors.

applications for artificial spinning of the fibrous silk materials. In HFIP medium the preferred molecular structure of the fibroin tends to be a 3_{10}-helix structure. The preliminary investigation also provides the characteristic ^{13}C-NMR chemical shifts data of the predominant Ala, Gly, and Ser residues of *B. mori* silk fibroin film prepared from HFIP system. The artificial spinning process of *B. mori* silk fibroin by HFIP system is proposed to undergo a distinct structural transition from a 3_{10}-helix to predominant β-sheet structure. Here, the Ala, Gly, and Ser residues located in the crystalline region of silk fibroin molecule are expected to play an important role during the transition process.

REFERENCES

1. Kuzuhara, A.; Asakura, T.; Tomoda, R.; Matsunaga, T. J Biotech 1987, 5, 199–207.
2. Asakura, T.; Kaplan, D. L. In Encyclopedia of Agricultural Science; Arutzen, C. J., Ed.; Academic Press: London, 1994; Vol 4, pp 1–11.
3. Demura, M.; Asakura, T.; Biotechnol Bioeng 1989, 33, 598–603.
4. Heslot, H. Biochimie 1998, 80, 19–31.
5. Demura, M.; Asakura, T.; Kuroo, T. Biosensors 1989, 4, 361–372.
6. Panitch, A.; Matsuki, K.; Cantor, E. J.; Cooper, S. J.; Atkins, E. D. T.; Fournier, M. J.; Mason, T. L.; Tirrell, D. A. Macromolecules 1997, 30, 42–49.
7. Cappello, J.; Crissman, J. W.; Dorman, M.; Mikolajczak, M.; Textor, G.; Marquet, M.; Ferrari, F. Biotechnol Prog 1990, 6, 198–202.
8. Winkler, S.; Szela, S.; Avtges, P.; Valluzzi, R.; Kirschner, D. A.; Kaplan, D. L. Int J Biol Macromol 1999, 24, 265–270.
9. Trabbic, K. A.; Yager, P. Macromolecules 1998, 31, 462–471.
10. Liivak, O.; Blye, A.; Shah, N.; Jelinski, L. W. Macromolecules 1998, 31, 2947–2951.
11. Lock, R. L. U.S. Patent 5,525,285, October 1993.
12. Yao, J.; Masuda, H.; Zhao, C.; Asakura. T. Macromolecules 2002, 35, 6–9.
13. Matsumoto, K.; Uejima, H.; Iwasaki, T.; Sano, Y.; Sumino, H. J Appl Polym Sci 1996, 60, 507–511.
14. Mathur, A. B.; Tonelli, A.; Rathke, T.; Hudson, S. Biopolymers 1997, 42, 61–74.
15. Seidel, A.; Liivak, O.; Calve, S.; Adaska, J.; Ji, G.; Yang, Z.; Grubb, D.; Zax, D. B.; Jelinski, L. W. Macromolecules 2000, 33, 775–780.
16. Asakura, T.; Sugino, R.; Yao, J.; Takashima, H.; Kishore, R. Biochemistry 2002, 41, 4415–4424.
17. Zhou, C.-Z.; Confalonieri, F.; Medina, N.; Zivanovic, Y.; Esnault, C.; Yang, T.; Jacquet, M.; Janin, J.; Duguet, M.; Perasso, R.; Li, Z.-G. Nucleic Acids Res 2000, 2, 2413–2419.
18. Asakura, T.; Kuzuhara, A.; Tabeta, R.; Saito, H. Macromolecules 1985, 18, 1841–1845.
19. Asakura, T.; Ito, T.; Okudaira, M.; Kameda, T. Macromolecules 1999, 32, 4940–4946.
20. Asakura, T.; Demura, M.; Date, T.; Miyashita, N.; Ogawa, K.; Williamson, M. P. Biopolymers 1997, 41, 193–203.
21. Asakura, T.; Watanabe, Y.; Uchida, A.; Minagawa, H. Macromolecules 1984, 17, 1075–1081.
22. Toniolo, C.; Polese, A.; Formaggio, F.; Crisma, M.; Kamphuis, J. J Am Chem Soc 1996, 118, 2744–2745.
23. Manning, M.; Woody, R. W. Biopolymers 1991, 31, 569–586.
24. Parrish, J. R., Jr.; Blout, E. R. Biopolymers 1972, 11, 1001–1020.
25. Kameda, T.; Ohkawa, Y.; Yoshizawa, K.; Nakano, E.; Hiraoki, T.; Ulrich, A. S.; Asakura, T. Macromolecules, 1999, 32, 8491–8495.
26. Asakura, T.; Yao, J.; Yamane, T.; Umemura, K.; Ulrich A. S. J Am Chem Soc 2002, 124, 8794–8795.
27. Asakura, T.; Yao, J. Protein Sci 2002, 11, 2706–2713.
28. Marsh, R. E.; Corey, R. B.; Pauling, L. Biochim Biophys Acta 1955, 16, 1–34.
29. Tsukada, M.; Obo, M.; Kato, H.; Freddi, G.; Zanetti, F. J Appl Polym Sci 1996, 60, 1619–1627.